IEEE TRANSACTIONS ON

ELECTROMAGNETIC COMPATIBILITY

A PUBLICATION OF THE IEEE ELECTROMAGNETIC COMPATIBILITY SOCIETY

EMC SOCIETY

NOVEMBER 2011 VOLUME 53 NUMBER 4 IEMCAE (ISSN 0018-9375)

(Contents Continued on Page 861)

IEEE

IEEE TRANSACTIONS ON ELECTROMAGNETIC COMPATIBILITY (ISSN 0018-9375) is published quarterly by the Institute of Electrical and Electronics Engineers, Inc. Responsibility for the contents rests upon the authors and not upon the IEEE, the Society/Council, or its members. **IEEE Corporate Office**: 3 Park Avenue, 17th Floor, New York, NY 10016-5997. **IEEE Operations Center:** 445 Hoes Lane, Piscataway, NJ 08854-4141. **NJ Telephone**: +1 732 981 0060. **Price/Publication Information:** Individual copies: IEEE Members $20.00 (first copy only), nonmembers $106.00 per copy. (Note: Postage and handling charge not included.) Member and nonmember subscription prices available upon request. **Copyright and Reprint Permissions**: Abstracting is permitted with credit to the source. Libraries are permitted to photocopy for private use of patrons, provided the per-copy fee indicated in the code at the bottom of the first page is paid through the Copyright Clearance Center, 222 Rosewood Drive, Danvers, MA 01923. For all other copying, reprint, or republication permission, write to Copyrights and Permissions Department, IEEE Publications Administration, 445 Hoes Lane, Piscataway, NJ 08854-4141.

Periodicals Postage Paid at New York, NY and at additional mailing offices. **Postmaster:** Send address changes to IEEE TRANSACTIONS ON ELECTROMAGNETIC COMPATIBILITY, IEEE, 445 Hoes Lane, Piscataway, NJ 08854-4141. GST Registration No. 125634188. CPC Sales Agreement #40013087. Return undeliverable Canada addresses to: Pitney Bowes IMEX, P.O. Box 4332, Stanton Rd., Toronto, ON M5W 3J4, Canada. IEEE prohibits discrimination, harassment and bullying. For more information visit http://www.ieee.org/nondiscrimination. Printed in U.S.A.

Digital Object Identifier 10.1109/TEMC.2011.2176159

Image and Exact Models of a Vertical Wire Penetrating a Two-Layered Earth

Vesna Arnautovski-Toseva, *Member, IEEE*, and Leonid Grcev, *Senior Member, IEEE*

***Abstract*—In this paper, we investigate the validity of image theory in modeling a vertical wire penetrating a uniform or two-layered earth. First, a rigorous full-wave electromagnetic model is described that may be used as a standard for comparison. The model is based on the method of moments (MoM) and exact Green functions for the layered earth that involve Sommerfeld-type integrals. Next, we derive the image model from the exact model and analyze the approximations. We compare the current along a vertical wire as computed by the MoM using the exact Green functions, with the current computed using the image Green functions. The image model is accurate at dc, and the error is generally low at low frequencies but rises at high frequencies. We show that the image model leads to smaller errors when the wire is embedded in one layer. However, the error is larger in cases of penetration through different layers. We also show a strong dependence of the error on the resonant frequencies.**

***Index Terms*—Antennas, electromagnetic analysis, frequency domain analysis, Green functions, grounding, modeling, nonhomogeneous media.**

I. Introduction

THE METHOD of images can be considered as a special case of the general electromagnetic equivalence theorem. In electrostatics, the validity of the image theory is firmly established because the boundary conditions are exactly met [1]. However, this is not generally the case in different variants of the method that are often used in electrodynamics. They are usually based on different approximate theories, although an exact image theory has also been introduced [2]. However, more accurate image theories commonly lead to more complicated numerical solutions that can hamper their practical applicability [3].

A fundamental application of the image method is to find image sources that can be defined as equivalent sources that replace physical structures, such as regions with different media. It is not a surprise that the image method is most often used to model the effects of the earth. Because the simplicity of the model is important for engineering analysis, simple images that can replace complex earth structures are often sought.

A simple model of the earth that enables an exact representation with images is a perfectly conducting earth with a planar surface (e.g., [4]). However, such a model generally cannot be used, e.g., in studies of grounding. The most usual model of the earth is a uniform or planar-layered lossy half-space. The images that replace such earth models are often extracted from electrostatics, where the image theory is exactly valid for dielectric layered media [5]. Due to the similarity between electrostatic and steady-current fields, the image theory is also valid for time-invariant point current sources in layered conducting media [6]. This is a well-known basis for the dc grounding analysis that is also approximately applied at 50/60 Hz [7].

The high frequency and transient performance of grounding systems have also been investigated in the last few decades. Different strategies for modeling have been developed ranging from simplified approaches based on circuit theory, with either lumped (e.g., [8], [9]) or distributed (e.g., [10], [11]) parameters, to rigorous approaches based on electromagnetic theory (e.g., [12], [13]). (A large body of literature is devoted to this subject; here, we mention only a few examples. The reader is referred to the reference sections of earlier papers by Grcev ([14], [15]) for useful information on recent work in this field.)

Importantly, effects of the earth's surface in the evaluation of the equivalent circuit parameters (both lumped and distributed) are usually determined by the static image theory (e.g., [9], [11]). On the other hand, the rigorous treatment of the air–earth interface in electromagnetic models ([12], [13]) is based on the exact solution for the field of a Hertz dipole near a conducting half-space that was first derived by Sommerfeld [16] and later summarized in the reference book by Banos [17]. However, this approach involves the time-consuming numerical integration of oscillatory and slowly convergent complex Sommerfeld integrals.

To circumvent this problem, recent modifications of the electromagnetic model have employed a simple variant of the image method based on the quasi-static image approximation of time-harmonic point current sources in lossy planar-layered media [6]. The method was used by Takashima *et al.* [18] for the high-frequency modeling of grounding electrodes; however, it has been shown in [19] that such modeling is limited to low frequencies. The method was later extended to high frequencies by Grcev [20] who used the same quasi-static reflection and refraction coefficients with a rigorous solution of the electromagnetic fields. More recently, this method has also been used for above-ground sources [21]. The simulation results of this

Manuscript received January 6, 2011; revised March 15, 2011; accepted April 20, 2011. Date of publication May 31, 2011; date of current version November 18, 2011. This work was supported in part by the FP7-PEOPLE-2009-IEF Project 253783, in part by the Republic of Macedonia Ministry of Education and Science, and in part by the Macedonian Academy of Sciences and Arts.

V. Arnautovski-Toseva is with the Laboratoire des Sciences et Matériaux pour l'Electronique et, d'Automatique (LASMEA), Blaise Pascal University, Clermont-Ferrand 63177, France, on leave from the Faculty of Electrical Engineering and Information Technologies, Saints Cyril and Methodius University, Skopje 1000, Macedonia (e-mail: vesna.arnautovski@lasmea.univ-bpclermont.fr).

L. Grcev is with the Macedonian Academy of Sciences and Arts, Skopje 1000, Macedonia, and also with the Faculty of Electrical Engineering and Information Technologies, Saints Cyril and Methodius University, Skopje 1000, Macedonia (e-mail: lgrcev@feit.ukim.edu.mk).

Digital Object Identifier 10.1109/TEMC.2011.2149533

approach have been successfully compared with available experimental data (e.g., [14], [20]), but only for buried conductors. Nevertheless, the validity domain of this approximate approach has never been analyzed in detail.

The objective of this paper is to investigate the validity of the image method applied to a vertical wire that is above, below, or penetrates a uniform or a two-layered earth. We consider only the simplest implementation of the image method. In this paper, we do not consider comparisons with more complex image models, such as discrete complex image models (e.g., [22]).

First, a full-wave rigorous electromagnetic model is described that may be used as a standard for comparison. Recently, such a model has been introduced by the authors for horizontal wires [23], and in this paper, we extend the model to vertical conductors. The model is based on the method of moments (MoM) [24] and exact Green functions for the two-layered earth. Next, we derive the image model from the rigorous model and identify the approximations introduced in the development. Finally, we compare the current along a vertical wire as computed by the MoM using the exact Green functions, with the current computed using the image Green functions for a range of frequencies from 10 kHz to 100 MHz.

To validate the proposed exact model, we compare our computation results with those by the other authors' models and commercial software, and we conclude that a fairly good agreement exists.

II. Exact Model

The analysis of electromagnetic fields and waves in stratified media has recently attracted much attention in different areas of research. The exact solution [16], [17], has been extended to arbitrary planar stratified media and has been used as an approximation in a myriad of practical applications (e.g., in above-ground and subsurface communications, radar, geophysical prospecting, bioelectromagnetics, microstrip circuits, and antennas) [26]–[32]. More recently, the research has focused on microstrip patch antennas, printed circuit boards, and monolithic microwave/millimeter-wave integrated circuits [33]–[36]. However, the majority of the research is related to dielectric media, where the problems in the numerical solution are considerably less involved than those for conductive media [23].

The details of the exact model for conductors in two-layered conductive media may be found in various places in the literature, e.g., [33]–[36]. Here, we briefly summarize the main steps in the development of the proposed model.

A. Mixed Potential Integral Equation and the MoM

The coordinate system is illustrated in Fig. 1. The interface between the air and the two-layered earth is the plane $z = 0$, with the positive z-direction upward into the air. The layers are denoted by 0 for the air, 1 for the earth's upper layer of finite depth d, and 2 for the earth's lower semi-infinite layer. The layers are characterized by corresponding values of permittivity ε_m and conductivity σ_m, $m = 0, 1, 2$, with $\sigma_0 = 0$. The permeability of the vacuum is assumed in all of the layers, i.e., $\mu_m = \mu_0$, $m = 0, 1, 2$. We consider a vertical wire of length ℓ

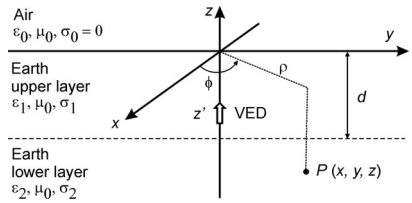

Fig. 1. Illustration of the coordinate system.

along the z-axis of the coordinate system that penetrates the planar three-layered medium. The wire excitation is provided by a harmonic voltage source. (The time variation $e^{j\omega t}$ is assumed and suppressed.)

By assuming the thin-wire approximation and applying appropriate boundary conditions for the electric field on the surface of the wire, the following well-known mixed potential integral equation can be derived [33], [35]:

$$E_z = -j\omega \int_\ell G_A I(z')dz' + \frac{1}{j\omega}\frac{d}{dz}\int_\ell G_V \frac{dI(z')}{dz'}dz' \quad (1)$$

where $I(z')$ is the unknown current along the axis of the wire. Here, G_A and G_V are the magnetic vector and electric scalar potential Green functions, respectively. In addition, $j = \sqrt{-1}$ and ω is the angular frequency. The right-hand side of (1) represents the tangential electric field due to all induced currents, and the left-hand side of (1) denotes the excitation by the impressed tangential electric field.

Equation (1) can be solved numerically by applying the MoM [24], which enables the reduction of (1) to a matrix equation

$$[Z]\cdot[I] = [V]\,. \quad (2)$$

First, it is assumed that the wire is divided into a number of fictitious short subsections that are connected. Next, the unknown current is approximated by a sequence of N expansion functions over the subsections. Here, we use roof-top functions T_i, which results in a piecewise linear approximation of the current. The boundary conditions regarding the tangential component of the electric field at the wire surface are satisfied approximately in an average (weighted) way. In a procedure that is referred to as the Galerkin method, we choose the weighting function to be the same roof-top functions T_j as the expansion functions [37]. The elements of the column matrix $[I]$ in (2) are complex numbers that represent the amplitudes of the corresponding current expansion functions, and the elements of $[V]$ in (2) are related to the excitation of the wire. The elements of the generalized impedance matrix $[Z]$ in (2) describe the electromagnetic interactions between subsections

$$z_{ij} = j\omega \int_{\ell_j} T_j dz \int_{\ell_i} G_A T_i dz' + \frac{1}{j\omega}\int_{\ell_j}\frac{dT_j}{dz}dz\int_{\ell_i} G_V \frac{dT_i}{dz'}dz'. \quad (3)$$

A voltage source that energizes the wire can be approximately represented by an element of $[V]$ in (2) [38].

To evaluate (3), it is necessary to determine G_A and G_V.

B. Green Functions in the Spectral Domain

By following the method described in [33]–[36], we first derive the Green functions in the spectral domain. In Fig. 1, we consider a Hertzian vertical electric dipole (VED) of unit strength ($Idz = 1\,\mathrm{Am}$) that is located at $(0,\,0,\,z')$, and pointed in the z-direction. The field is observed in *P* at $(x,\,y,\,z)$. The regions where the VED and *P* are located are denoted by *m* and *n*, respectively, where $m,\,n = 0, 1,\,2$.

Here, we present the expressions of the Green functions only for two characteristic cases: first, when both the VED and *P* are in the upper earth layer, i.e., when $m = n = 1$, and second, when the VED is in region $m = 1$ and *P* is in region $n = 0$. The Green functions in other cases can be similarly determined.

1) VED and P in Region 1: Spectral expressions for the magnetic vector potential Green function $\tilde{G}_A^{11}$ and the electric scalar potential Green function $\tilde{G}_V^{11}$ can be written in the following form:

$$\tilde{G}_A^{11} = (\tilde{G}_A^{11})_d + (\tilde{G}_A^{11})_r \tag{4}$$

$$\tilde{G}_V^{11} = (\tilde{G}_V^{11})_d + (\tilde{G}_V^{11})_r \tag{5}$$

where

$$(\tilde{G}_A^{11})_d = \frac{\mu_0}{2}\frac{e^{-jk_{z1}|z-z'|}}{jk_{z1}}$$

$$(\tilde{G}_A^{11})_r = \frac{\mu_0}{2}\left[A\frac{e^{jk_{z1}|z|}}{jk_{z1}} + B\frac{e^{-jk_{z1}|z|}}{jk_{z1}}\right] \tag{6}$$

$$(\tilde{G}_V^{11})_d = \frac{1}{2\underline{\varepsilon}_1}\frac{e^{-jk_{z1}|z-z'|}}{jk_{z1}},$$

$$(\tilde{G}_V^{11})_r = \frac{1}{2\underline{\varepsilon}_1}\left[C\frac{e^{jk_{z1}|z|}}{jk_{z1}} + D\frac{e^{-jk_{z1}|z|}}{jk_{z1}}\right] \tag{7}$$

$$k_{z1} = \sqrt{k_1^2 - k_\rho^2}, \quad k_\rho = \sqrt{k_x^2 + k_y^2}$$

$$k_1 = \omega\sqrt{\mu_0\underline{\varepsilon}_1}, \quad \underline{\varepsilon}_1 = \varepsilon_1 - j\sigma_1/\omega.$$

Here,

$$A = e^{-jk_{z1}d}R_{12}M\left[e^{-jk_{z1}(d-|z'|)} + R_{10}e^{-jk_{z1}(d+|z'|)}\right]$$

$$B = R_{10}M\left[e^{-jk_{z1}|z'|} + R_{12}e^{-jk_{z1}(2d-|z'|)}\right]$$

$$C = e^{-jk_{z1}d}R_{12}M\left[-e^{-jk_{z1}(d-|z'|)} + R_{10}e^{-jk_{z1}(d+|z'|)}\right]$$

$$D = R_{10}M\left[-e^{-jk_{z1}|z'|} + R_{12}e^{-jk_{z1}(2d-|z'|)}\right] \tag{8}$$

$$M = \left(1 - R_{10}R_{12}e^{-jk_{z1}2d}\right)^{-1} \tag{9}$$

where R_{mn} are the Fresnel reflection coefficients [31]

$$R_{10} = \frac{\varepsilon_0 k_{z1} - \underline{\varepsilon}_1 k_{z0}}{\varepsilon_0 k_{z1} + \underline{\varepsilon}_1 k_{z0}}, \quad R_{12} = \frac{\underline{\varepsilon}_2 k_{z1} - \underline{\varepsilon}_1 k_{z2}}{\underline{\varepsilon}_2 k_{z1} + \underline{\varepsilon}_1 k_{z2}}. \tag{10}$$

In (4)–(7), the terms $(\tilde{G})_d$ are the Green functions of the VED in an unbounded medium with the characteristics of the field observation region (here, $n = 1$). Also, the terms $(\tilde{G})_r$ correspond to the upward and downward waves that are reflected from the interfaces.

In the case of a homogeneous earth, the coefficient $R_{12} = 0$, which leads to a simplification of the reflection terms in (6) and (7)

$$(\tilde{G}_A^{11})_r = \frac{\mu_0}{2}R_{10}\frac{e^{-jk_{z1}|z+z'|}}{jk_{z1}} \quad \text{and}$$

$$(\tilde{G}_V^{11})_r = \frac{-1}{2\underline{\varepsilon}_1}R_{10}\frac{e^{-jk_{z1}|z+z'|}}{jk_{z1}}. \tag{11}$$

2) VED in Region 1 and P in Region 0: If the VED is in region 1 and the field observation point *P* is in region 0, $\tilde{G}_A^{10}$ and $\tilde{G}_V^{10}$ can be written in the following form:

$$\tilde{G}_A^{10} = \frac{\mu_0}{2}T_{10}Me^{-jk_{z0}z}\left[\frac{e^{-jk_{z1}|z'|}}{jk_{z1}} + R_{12}\frac{e^{-jk_{z1}(2d-|z'|)}}{jk_{z1}}\right] \tag{12}$$

$$\tilde{G}_V^{10} = \frac{1}{2\varepsilon_0}MT_{10}\frac{k_{z0}}{k_{z1}}e^{-jk_{z0}z}\left[\frac{e^{-jk_{z1}|z'|}}{jk_{z1}} - R_{12}\frac{e^{-jk_{z1}(2d-|z'|)}}{jk_{z1}}\right] \tag{13}$$

where T_{mn} are the Fresnel transmission coefficients [31]

$$T_{10} = 1 + R_{10}, \quad T_{12} = 1 + R_{12}. \tag{14}$$

In the case of a homogeneous earth, the coefficient $T_{12} = 0$, which leads to a simplification of the expressions (12) and (13)

$$\tilde{G}_A^{10} = \frac{\mu_0}{2}T_{10}e^{-jk_{z0}z}\frac{e^{-jk_{z1}|z'|}}{jk_{z1}}$$

$$\text{and} \quad \tilde{G}_V^{10} = \frac{1}{2\varepsilon_0}T_{10}\frac{k_{z0}}{k_{z1}}e^{-jk_{z0}z}\frac{e^{-jk_{z1}|z'|}}{jk_{z1}}. \tag{15}$$

C. Green Functions in the Spatial Domain

The spatial expressions for G_A^{mn} and G_V^{mn} can be determined by means of the 2-D inverse Fourier transform of their spectral pairs, $\tilde{G}_A^{mn}$ and $\tilde{G}_V^{mn}$, respectively, which leads to the well-known Sommerfeld integral [35]

$$G_{A,V}^{mn} = S_0\left\{\tilde{G}_{A,V}^{mn}\right\} = \frac{1}{2\pi}\int_0^\infty \tilde{G}_{A,V}^{mn}J_0(k_\rho\rho)k_\rho dk_\rho \tag{16}$$

where $J_0(k_\rho\rho)$ is a zero-order Bessel function of the first kind, and $\rho = \sqrt{x^2 + y^2}$ is the radial distance between the VED and field evaluation point.

Here, we present the spatial expressions of the Green functions that correspond to the case when both the VED and the field point are in the region $m = n = 1$

$$G_A^{11} = S_0\left\{(\tilde{G}_A^{11})_d\right\} + S_0\left\{(\tilde{G}_A^{11})_r\right\} \tag{17}$$

$$G_V^{11} = S_0\left\{(\tilde{G}_V^{11})_d\right\} + S_0\left\{(\tilde{G}_V^{11})_r\right\}. \tag{18}$$

The first terms in (17) and (18), i.e., $S_0\{(\tilde{G}_A^{11})_d\}$ and $S_0\{(\tilde{G}_V^{11})_d\}$, respectively, have closed-form solutions

$$S_0\{(\tilde{G}_A^{11})_d\} = (G_A^{11})_d = \frac{\mu_0}{4\pi}g_d^1 \tag{19}$$

$$S_0\{(\tilde{G}_V^{11})_d\} = (G_V^{11})_d = \frac{1}{4\pi\underline{\varepsilon}_1} g_d^1 \tag{20}$$

$$g_d^1 = \frac{e^{-jk_1 r}}{r}, \quad r = \sqrt{\rho^2 + |z - z'|^2}.$$

Here, g_d^1 in (19) and (20) are related to a spherical wave due to VED in an unbounded medium with characteristics of the region $n = 1$, i.e., with propagation wavenumber k_1.

However, the second terms in (17) and (18) have no analytical solutions. It is also the case with G_A^{10} and G_V^{10} when the VED is in region $m = 1$ and the field observation point is in region $n = 0$ that

$$G_A^{10} = S_0\left\{\tilde{G}_A^{10}\right\} \text{ and } G_V^{10} = S_0\left\{\tilde{G}_V^{10}\right\}. \tag{21}$$

We determined the second terms in (17) and (18), as well as the expressions in (21), by direct numerical integration in a similar way to the approach used by Burke and Miller [25].

III. Image Model

Similarly, as in the previous section, we present the image Green functions only for the characteristic cases: first, when both the VED and *P* are in the upper earth layer, i.e., when $m = n = 1$; and second, when the VED is in region $m = 1$ and *P* is in region $n = 0$. The image Green functions in other cases can be similarly determined.

1) VED and P in Region 1: The image model is accurate for dc Hertz dipoles [40]. We look for an approximate solution valid at low frequencies. If $\omega \to 0$ and $k_0 \to 0$, then $k_{z0} \approx k_{z1} \approx k_{z2}$ in the spectral domain because $k_\rho^2 >> k_n^2$ for $n = 0, 1, 2$. By substitution in (10), we come to the following low-frequency approximation of the reflection coefficients:

$$R_{mn} \to -R_{mn}^{\mathrm{QS}} = -\frac{\underline{\varepsilon}_m - \underline{\varepsilon}_n}{\underline{\varepsilon}_m + \underline{\varepsilon}_n}. \tag{22}$$

This leads to key simplifications because R_{mn}^{QS} is a constant in the spectral domain and can be extracted from the integrals, which enables the derivation of closed-form solutions of the integrals. Notably, R_{mn}^{QS} is equivalent to the quasi-static reflection coefficient applied in [18].

Next, we substitute (22) into (8), which allows one to rewrite and expand the term *M* in the following series [26]:

$$M \to \left(1 - R_{10}^{\mathrm{QS}} R_{12}^{\mathrm{QS}} e^{-jk_{z1}2d}\right)^{-1} \approx \sum_{p=0}^{\infty} (R_{10}^{\mathrm{QS}} R_{12}^{\mathrm{QS}})^p e^{-jk_{z1}2dp}. \tag{23}$$

This approximation enables the transformation of (8) by

$$\begin{aligned} A &\approx -R_{12}^{\mathrm{QS}} \left[e^{-jk_{z1}(2d-|z'|)} - R_{10}^{\mathrm{QS}} e^{-jk_{z1}(2d+|z'|)}\right] \\ &\quad \times \sum_{p=0}^{\infty} (R_{10}^{\mathrm{QS}} R_{12}^{\mathrm{QS}})^p e^{-jk_{z1}2dp} \\ B &\approx -R_{10}^{\mathrm{QS}} \left[e^{-jk_{z1}|z'|} - R_{12}^{\mathrm{QS}} e^{-jk_{z1}(2d-|z'|)}\right] \\ &\quad \times \sum_{p=0}^{\infty} (R_{10}^{\mathrm{QS}} R_{12}^{\mathrm{QS}})^p e^{-jk_{z1}2dp} \\ C &\approx R_{12}^{\mathrm{QS}} \left[e^{-jk_{z1}(2d-|z'|)} + R_{10}^{\mathrm{QS}} e^{-jk_{z1}(2d+|z'|)}\right] \\ &\quad \times \sum_{p=0}^{\infty} (R_{10}^{\mathrm{QS}} R_{12}^{\mathrm{QS}})^p e^{-jk_{z1}2dp} \\ D &\approx R_{10}^{\mathrm{QS}} \left[e^{-jk_{z1}|z'|} + R_{12}^{\mathrm{QS}} e^{-jk_{z1}(2d-|z'|)}\right] \\ &\quad \times \sum_{p=0}^{\infty} (R_{10}^{\mathrm{QS}} R_{12}^{\mathrm{QS}})^p e^{-jk_{z1}2dp}. \end{aligned} \tag{24}$$

Next, we substitute (24) into (17), by which $S_0\{(\tilde{G}_A^{11})_r\}$ in (17) may be rewritten as

$$\begin{aligned} S_0\{(\tilde{G}_A^{11})_r\} \to \frac{\mu_0}{2} \Bigg[&-R_{12}^{\mathrm{QS}} \sum_{p=1}^{\infty} (R_{12}^{\mathrm{QS}} R_{10}^{\mathrm{QS}})^{p-1} S_0\left\{\frac{e^{-jk_{z1}h_{1p}}}{jk_{z1}}\right\} \\ &+ \sum_{p=1}^{\infty} (R_{12}^{\mathrm{QS}} R_{10}^{\mathrm{QS}})^p S_0\left\{\frac{e^{-jk_{z1}h_{2p}}}{jk_{z1}}\right\} \\ &- R_{10}^{\mathrm{QS}} S_0\left\{\frac{e^{-jk_{z1}|z+z'|}}{jk_{z1}}\right\} \\ &- R_{10}^{\mathrm{QS}} \sum_{p=1}^{\infty} (R_{12}^{\mathrm{QS}} R_{10}^{\mathrm{QS}})^p S_0\left\{\frac{e^{-jk_{z1}h_{3p}}}{jk_{z1}}\right\} \\ &+ \sum_{p=1}^{\infty} (R_{12}^{\mathrm{QS}} R_{10}^{\mathrm{QS}})^p S_0\left\{\frac{e^{-jk_{z1}h_{4p}}}{jk_{z1}}\right\}\Bigg] \\ h_{1p} = 2pd - |z'| + z, &\quad h_{2p} = 2pd + |z'| + z \\ h_{3p} = 2pd + |z'| - z, &\quad h_{4p} = 2pd - |z'| - z. \end{aligned} \tag{25}$$

The Sommerfeld integrals in (25) have the closed-form solutions

$$S_0\left\{\frac{e^{-jk_{z1}h_{lp}}}{jk_{z1}}\right\} = \frac{1}{2\pi}\int_0^{\infty} \frac{e^{-jk_{z1}h_{lp}}}{jk_{z1}} J_0(k_\rho\rho) k_\rho dk_\rho = \frac{1}{2\pi} g_{lp}^1$$

$$g_{lp}^1 = \frac{e^{-jk_1 r_{lp}}}{r_{lp}}, \quad r_{lp} = \sqrt{\rho^2 + h_{lp}^2}, \quad l = 1, 2, 3, 4. \tag{26}$$

Each of the g_{lp}^1 terms is related to the field of an image source. Finally, we obtain the following image approximation of (17):

$$\begin{aligned} G_A^{11} \approx \frac{\mu_0}{4\pi} \Bigg\{ &g_d^1 - R_{10}^{\mathrm{QS}} g_0^1 \\ &+ \sum_{p=1}^{\infty} (R_{10}^{\mathrm{QS}} R_{12}^{\mathrm{QS}})^p \left[-\frac{1}{R_{10}^{\mathrm{QS}}} g_{1p}^1 + g_{2p}^1 - R_{10}^{\mathrm{QS}} g_{3p}^1 + g_{4p}^1\right]\Bigg\} \end{aligned} \tag{27}$$

$$g_0^1 = \frac{e^{-jk_1 r_0}}{r_0}, \quad r_0 = \sqrt{\rho^2 + (z + z')^2}$$

where g_d^1 is given in (19) and g_{lp}^1 is given in (26).

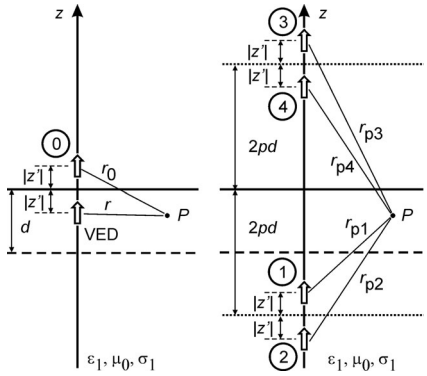

Fig. 2 Image positions when both the VED and field evaluation point *P* are in the same layer. (a) VED and zeroth image. (b) Group of four images.

Similarly, we obtain the image approximation of (18)

$$G_V^{11} \approx \frac{1}{4\pi\underline{\varepsilon}_1}\left\{g_d^1 + R_{10}^{\mathrm{QS}} g_0^1 + \sum_{p=1}^{\infty}(R_{10}^{\mathrm{QS}} R_{12}^{\mathrm{QS}})^p \left[\frac{1}{R_{10}^{\mathrm{QS}}} g_{1p}^1 + g_{2p}^1 + g_{3p}^1 + R_{10}^{\mathrm{QS}} g_{4p}^1\right]\right\}. \tag{28}$$

The image representations in (27) and (28) are illustrated in Fig. 2. The first two terms in brackets in (27) and (28) are related to the original VED (g_d^1) and the zeroth image (g_0^1), respectively, which are illustrated in Fig. 2(a). The terms within the sum in (27) and (28) ($g_{lp}^1,\ l = 1, 2, 3, 4,\ p = 1, 2, \ldots, \infty$) are related to the set of four images of the *p*th series that are obtained with respect to both boundaries, as shown in Fig. 2(b). Therefore, the layered media are replaced by a homogeneous medium with the characteristics of layer 1 and an infinite series of image sources positioned along the positive and negative sides of the z-axis.

In the case of a homogeneous earth, the coefficient $R_{12}^{\mathrm{QS}} = 0$ and image expressions (27) and (28) are simplified as

$$G_A^{11} \approx \frac{\mu_0}{4\pi}\left\{g_d^1 - R_{10}^{\mathrm{QS}} g_0^1\right\}, \quad G_V^{11} \approx \frac{1}{4\pi\underline{\varepsilon}_1}\left\{g_d^1 + R_{10}^{\mathrm{QS}} g_0^1\right\}. \tag{29}$$

The images that replace the homogenous earth are illustrated only in Fig. 2(a).

2) VED in Region 1 and P in Region 0: As a consequence of the approximation in (22), it follows that the transmission coefficients (14) are approximated by

$$T_{mn} \to T_{mn}^{\mathrm{QS}} = \frac{2\underline{\varepsilon}_n}{\underline{\varepsilon}_n + \underline{\varepsilon}_m} = 1 - R_{mn}^{\mathrm{QS}}. \tag{30}$$

Substituting (22) and (30) into (12) leads to the following approximation of G_A^{10}:

$$G_A^{10} \to \frac{\mu_0}{2} T_{10}^{\mathrm{QS}} \sum_{p=0}^{\infty}(R_{10}^{\mathrm{QS}} R_{12}^{\mathrm{QS}})^p \times \left[S_0\left\{\frac{e^{-jk_{z0}h_{1p}}}{jk_{z0}}\right\} + R_{12}^{\mathrm{QS}} S_0\left\{\frac{e^{-jk_{z2}h_{2p}}}{jk_{z0}}\right\}\right]. \tag{31}$$

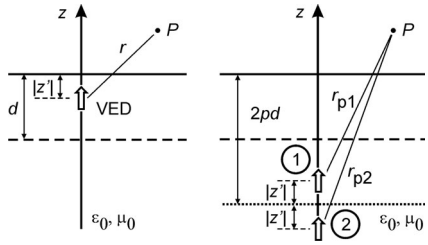

Fig. 3. Image positions when the VED is in region 1 and the field evaluation point *P* is in region 0. (a) Modified VED. (b) Group of two images.

The Sommerfeld integrals in (31) have the closed-form solutions given in (26) that lead to the following image approximation:

$$G_A^{10} \approx \frac{\mu_0}{4\pi} \times \left\{T_{10}^{\mathrm{QS}} g_d^0 + T_{10}^{\mathrm{QS}} \sum_{p=1}^{\infty}(R_{10}^{\mathrm{QS}} R_{12}^{\mathrm{QS}})^p \left[g_{1p}^0 - \frac{1}{R_{10}^{\mathrm{QS}}} g_{2p}^0\right]\right\}. \tag{32}$$

Similarly, we obtain the image approximation of G_V^{10}:

$$G_V^{10} \approx \frac{1}{4\pi\varepsilon_0} \times \left\{T_{10}^{\mathrm{QS}} g_d^0 + T_{10}^{\mathrm{QS}} \sum_{p=1}^{\infty}(R_{10}^{\mathrm{QS}} R_{12}^{\mathrm{QS}})^p \left[g_{1p}^0 + \frac{1}{R_{10}^{\mathrm{QS}}} g_{2p}^0\right]\right\}. \tag{33}$$

The images in (32) and (33) are illustrated in Fig. 3. The first term in brackets in (32) and (33) is related to the original VED (g_d^0), as shown in Fig. 3(a). The terms within the sum in (32) and (33) ($g_{lp}^0,\ l = 1, 2,\ p = 1, 2, \ldots, \infty$) are related to the set of two images of the *p*th series that are obtained with respect to both boundaries, as shown in Fig. 2(b). Notably, the position of the images in Fig. 3(b) is the same as the corresponding images in Fig. 2(b) (denoted by $p = 1, 2$). Therefore, in this case, the layered media are replaced by a homogeneous medium with the characteristics of layer 0 (the layer where the field observation point *P* is positioned) with an infinite series of image sources positioned along the negative side of the z-axis.

In the case of a homogeneous earth, the coefficient $R_{12}^{QS} = 0$ and image expressions (32) and (33) are simplified by

$$G_A^{10} = \frac{\mu_0}{4\pi} T_{10}^{\mathrm{QS}} g_d^0, \quad G_V^{10} = \frac{1}{4\pi\varepsilon_0} T_{10}^{\mathrm{QS}} g_d^0. \tag{34}$$

This case is illustrated in Fig. 3(a).

Finally, if we assume $\omega = 0$, we obtain $R_{10}^{\mathrm{QS}} \to 1$ and $e^{-jk_n r} \to 1$, and expressions (27) and (28), and (32) and (33) reduce to static images [40].

IV. Validation of the Exact Model

First, in Fig. 4, we compare the proposed exact model results with data published in [25]. The test case is a quarter-wave

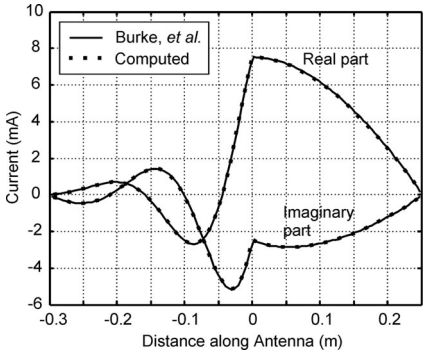

Fig. 4. Comparison of the proposed exact model with that of Burke and Miller [25].

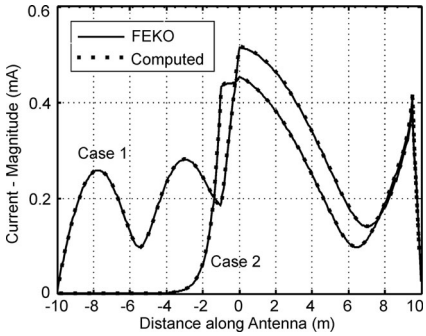

Fig. 5. Comparison of the proposed exact model with FEKO [39]. Case 1: $\sigma_1/\sigma_2 = 0.01$ S/m/0.001 S/m. Case 2: $\sigma_1/\sigma_2 = 0.01$ S/m/0.1 S/m.

antenna that penetrates a uniform earth. The length of the aerial part is 0.25 m with a ground stake of 0.3 m and a radius of 0.25 mm. A harmonic voltage excitation with an rms amplitude of 1 V was assumed at $z = 0$. The calculations are performed at 300 MHz (which corresponds to a 1-m wavelength in air). The conductivity of the earth is $\sigma = 0.267$ S/m, and the relative dielectric constant is set to 16 to match $\underline{\varepsilon} = (16 - j16)$, [25, Fig. 3]. The computed results are consistent with those published in [25].

Next, in Fig. 5, we compare the exact model results for the two-layered earth model with the results from the commercial electromagnetic simulation software FEKO, which also uses an MoM-based full-wave solution of Maxwell's integral equations in the frequency domain with special Green functions for planar multilayered media [39]. The chosen test case is a vertical antenna with a 10-m-long aerial part that extends 10 m into the two-layered earth. The depth of the upper earth layer is 1 m. The presented comparison considers two cases: the conductivity of the upper earth layer is the same in both cases ($\sigma_1 = 0.01$ S/m), while those of the lower layer in the first and second cases is $\sigma_2 = 0.001$ and 0.1 S/m, respectively (see Fig. 5). The relative permittivity of all earth layers is 10. A voltage source of 1 V is placed at 9.5 m above the ground. The results that were computed with the proposed exact model are consistent with those computed by FEKO [39].

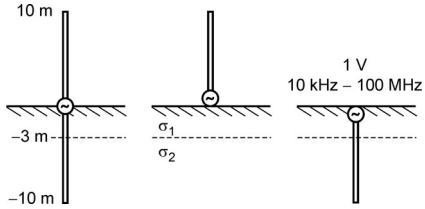

Fig. 6. Geometries of the test cases for the comparison studies.

TABLE I
EARTH PARAMETERS OF THE TEST CASES

Earth type	No. of layers	Earth conductivity (S/m)
A	2	σ_1/σ_2 = 0.01/0.001
B	2	σ_1/σ_2 = 0.001/0.01
H1	1	σ = 0.01
H2	1	σ = 0.001

V. COMPARISON OF THE IMAGE AND EXACT MODELS

A. Computation Test Cases

The geometry of the test cases is illustrated in Fig. 6. The wire is constructed of copper, and in all cases in Fig. 6, 10 m of the wire is in the air and 10 m is in the ground. (The total length of the wire in the case in Fig. 6(a) is 20 m.) The wire touches the surface of the earth in the cases in Fig. 6(a) and (b). The radius of the wire is 0.7 cm.

A harmonic voltage excitation of 1 V is assumed in a frequency range from 10 kHz to 100 MHz. The positions of the voltage source are the following: case (a), at the surface of the earth ($z = 0$); case (b), at ($z = 0.25$ m); and case (c), at ($z = -0.25$ m).

Four distinct sets of earth parameters are considered, as given in Table I. In all cases, the relative permittivity of the earth is 10.

To compare the image and exact models, we computed the following scalar parameter, which is referred to as the normalized rms error [41]:

$$(\varepsilon_S)_{\mathrm{rms}} = \left[\frac{\sum_{k=1}^{N} |\underline{I}_{Ek} - \underline{I}_{Ik}|^2}{\sum_{k=1}^{N} |\underline{I}_{Ek}|^2}\right]^{\frac{1}{2}} \times 100 \quad (\%) \qquad (35)$$

where $\underline{I}_{Ek}$ and $\underline{I}_{Ik}$, $k = 1, 2, \ldots, N$, are the phasors of the current samples along the segments of the wire as computed by the MoM when using the exact and image Green functions, respectively, and N is the number of segments.

B. Wire Penetrates Earth

Figs. 7 and 8 show the rms error $(\varepsilon_S)_{\mathrm{rms}}$ (35) of the current along a wire that penetrates the earth as computed by the image model with the exact model as a reference. The results in Fig. 7 are for a uniform earth and, in Fig. 8, for a two-layered earth. We see that the image model is a low-frequency approximation that leads to errors in the currents smaller than 1% at frequencies smaller than 10 kHz, but the error increases with the frequency and becomes about 10% to 15% at frequencies near 10 MHz.

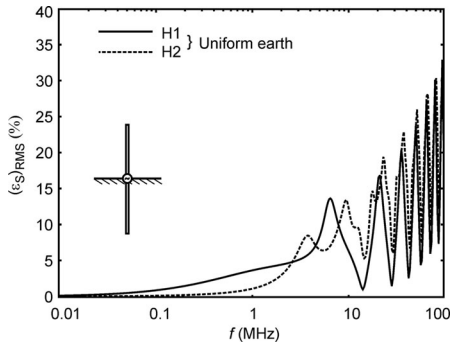

Fig. 7. Error in the current along a wire penetrating the earth as computed by the image model. The geometry is given in Fig. 6(a). The uniform earth parameters are given in Table I.

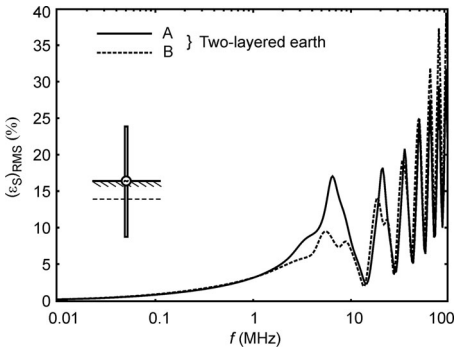

Fig. 8. Error in the current along a wire penetrating the earth computed by the image model. The geometry is given in Fig. 6(a). The two-layered earth parameters are given in Table I.

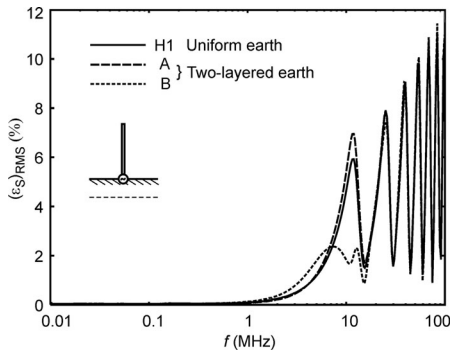

Fig. 9. Error in the current along a wire above the earth as computed by the image model. The geometry is given in Fig. 6(b). The earth parameters are given in Table I.

In this frequency range, the error depends on the earth's conductivity and is smaller for a less conductive earth. However, at frequencies above approximately 10 MHz, the error is strongly dependent on the resonances. The values of the error oscillate between minima of a few percent to maxima on the order of ten times higher (see Figs. 7 and 8). In this high-frequency range, the influence of the characteristics of the earth is not large, and all the error curves in Figs. 8 and 9 follow a similar pattern.

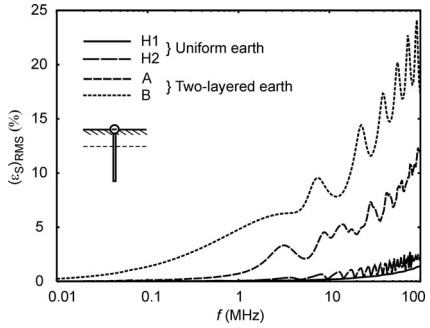

Fig. 10. Error in the current along a wire below the earth as computed by the image model. The geometry is given in Fig. 6(c). The earth parameters are given in Table I.

C. Wire Above the Earth

Fig. 9 shows the rms error $(\varepsilon_S)_{\rm rms}$ (35) of the current along a wire that is completely in the air. In this case, in which there is no penetration of the wire through the earth surface, the error is smaller than in the case described in the previous section. The values of the error are less than 1% up to frequencies of about 1 MHz, and the maximal values of the error are within a limit of about 10%, even at resonant frequencies up to 100 MHz, as shown in Fig. 9.

D. Wire Buried in Earth

Fig. 10 shows the rms error $(\varepsilon_S)_{\rm rms}$ (35) of the current along a wire that is completely buried in the earth. In this case, we can distinguish two scenarios: first, when the wire is buried in the uniform earth and, second, when it is buried in the layered earth. The error is small (less than about 2%) throughout the entire frequency range (up to 100 MHz) when the wire is buried in the uniform earth, i.e., when there is no penetration through different media.

However, in the case of a buried wire that penetrates different earth layers, the values of the error are larger both at low and high frequencies, with maxima at resonant frequencies approaching up to 25%, as shown in Fig. 10.

In the case (not shown here) where a wire (2.5 m long) is embedded in the upper layer, i.e., when there is no penetration through different media, the values of the error are particularly small (less than 1%) throughout the entire frequency range up to 100 MHz.

E. Discussion

The resonant behaviors of the errors in Figs. 7–10 follow the resonant behavior of the wire, and the error is maximal at the resonant frequencies. In general, the resonant frequencies are dependent on the geometry and characteristics of the medium, but in the cases in Figs. 7–9 in the frequency range above 10 MHz, they can be roughly approximated by [42]

$$f = \frac{1}{2\sqrt{\varepsilon_0 \mu_0}} \frac{n}{\ell} \tag{36}$$

where $n = 1, 3, 5, ...$, in Figs. 7 and 8 and $n = 1, 2, 3, ...$, in Fig. 9.

Our future work on the improvement of the presented image model will focus on the improvement of the error near the resonant frequencies and in cases when the wire penetrates different media.

VI. Conclusion

In this paper, we have compared the image and exact models of a wire that is above, below, or penetrates a uniform or two-layered earth. The image model can be derived from the exact model by a single substitution of the reflection Fresnel coefficients in the spectral domain with their quasi-static forms.

The image model is accurate at dc and leads to generally small errors at low frequencies and larger errors at higher frequencies. At frequencies above 10 MHz, the error is strongly dependent on the resonant frequencies.

The error is smaller when there is no penetration of the wire through different media. The error is small (less than a few percent in the frequency range up to 100 MHz) for a wire buried in a uniform earth and even smaller (less than one percent) if the wire is embedded in the upper layer of the two-layered earth. The error is larger, but still within a limit of about 10%, in the case of a wire completely above the ground.

The error is largest in cases where the wire penetrates different media. In such cases, the error is larger than that observed for a wire in uniform media, both at low and at high frequencies, and attains values of about 40% at resonant frequencies.

References

[1] Z. Popovic and B. Popovic, *Introductory Electromagnetics*. Upper Saddle River, NJ: Prentice-Hall, 2000.

[2] I. V. Lindell, *Methods for Electromagnetic Field Analysis*. New York: Wiley-IEEE, 1992.

[3] I. V. Lindell, "On the integration of image sources in exact image method of field analysis," *J. Electromagn. Waves Appl.*, vol. 2, no. 7, pp. 607–619, 1988.

[4] Y. Baba and V. A. Rakov, "Electric and magnetic fields predicted by different electromagnetic models of the lightning return stroke versus measured fields," *IEEE Trans. Electromagn. Compat.*, vol. 51, no. 3, pp. 479–487, Aug. 2009.

[5] S. A. Schelkunoff, *Electromagnetic Waves*. New York: Van Nostrand, 1943.

[6] J. R. Wait, *Electromagnetic Wave Theory*. New York: Harper & Row, 1985.

[7] G. F. Tagg, *Earth Resistances*. London, U.K.: G. Newnes, 1964.

[8] R. Rudenberg, *Electrical Shock Waves in Power Systems*. Cambridge, MA: Harvard Univ. Press, 1968.

[9] A. Geri, "Behaviour of grounding systems excited by high impulse currents: The model and its validation," *IEEE Trans. Power Del.*, vol. 14, no. 3, pp. 1008–1017, Jul. 1999.

[10] E. D. Sunde, *Earth Conduction Effects in Transmission Systems*, 2nd ed. ed. New York: Dover, 1968.

[11] Y. Liu, M. Zitnik, and R. Thottappillil, "An improved transmission-line model of grounding system," *IEEE Trans. Electromagn. Compat.*, vol. 3, no. 3, pp. 348–355, Aug. 2001.

[12] D. Roubertou, J. Fontaine, J. P. Plumey, and A. Zeddam, "Harmonic input impedance of earth connections," in *Proc. IEEE Int. Symp. Electromagn. Compat.*, 1984, pp. 717–720.

[13] L. Grcev and F. Dawalibi, "An electromagnetic model for transients in grounding systems," *IEEE Trans. Power Del.*, vol. 5, no. 4, pp. 1773–1781, Oct. 1990.

[14] L. Grcev, "Time- and frequency-dependent lightning surge characteristics of grounding electrodes," *IEEE Trans. Power Del.*, vol. 24, no. 4, pp. 2186–2196, Oct. 2009.

[15] L. Grcev, "Modeling of grounding electrodes under lightning currents," *IEEE Trans. Electromagn. Compat.*, vol. 51, no. 3, pp. 559–571, Aug. 2009.

[16] A. Sommerfeld, *Partial Differential Equations in Physics*. New York: Academic, 1949.

[17] A. Banos, *Dipole Radiation in the Presence of a Conducting Half-Space*. Oxford: Pergamon, 1966.

[18] T. Takashima, T. Nakae, and R. Ishibashi, "High frequency characteristics of impedances to ground and field distributions of ground electrodes," *IEEE Trans. Power App. Syst.*, vol. 100, no. 4, pp. 1893–1900, Apr. 1980.

[19] L. Grcev, "Computation of transient voltages near complex grounding systems caused by lightning currents," in *Proc. IEEE Int. Symp. Electromagn. Compat.*, 1992, pp. 393–400.

[20] L. Grcev, "Computer analysis of transient voltages in large grounding systems," *IEEE Trans. Power Del.*, vol. 11, no. 2, pp. 815–823, Apr. 1996.

[21] A. Shoory, R. Moini, S. H. H. Sadeghi, and V. A. Rakov, "Analysis of lightning-radiated electromagnetic fields in the vicinity of lossy ground," *IEEE Trans. Electromagn. Compat.*, vol. 47, no. 1, pp. 131–145, Feb. 2005.

[22] A. Shoory, R. Moini, and S. H. H. Sadeghi, "Direct use of discrete complex image method for evaluating electric field expressions in a lossy half space," *IET Microw. Antennas Propag.*, vol. 4, no. 2, pp. 258–268, 2010.

[23] V. Arnautovski-Toseva and L. Grcev, "Electromagnetic analysis of horizontal wire in two-layered soil," *J. Comput. Appl. Math.*, vol. 168, nos. 1–2, pp. 21–29, Jul. 2004.

[24] R. F. Harrington, *Field Computation by Moment Method*. New York: Wiley-IEEE, 1993.

[25] G. J. Burke and E. K. Miller, "Modeling antennas near to and penetrating a lossy interface," *IEEE Trans. Antennas Propag.*, vol. 32, no. 10, pp. 1040–1049, Oct. 1984.

[26] L. M. Brekhovskikh, *Waves in Layered Media*. New York: Academic, 1960.

[27] J. R. Wait, *Electromagnetic Waves in Stratified Media*. Oxford, U.K.: Pergamon, 1962.

[28] J. A. Kong, *Electromagnetic Wave Theory*. New York: Wiley, 1975.

[29] R. W. P. King and G. S. Smith, *Antennas in Matter*. Cambridge, MA: MIT Press, 1981.

[30] V. W. Hansen, *Numerical Solution of Antennas in Layered Media*. New York: Wiley, 1989.

[31] W. C. Chew, *Waves and Fields in Inhomogeneous Media*. New York: Wiley–IEEE, 1995.

[32] K. Li, *Electromagnetic Fields in Stratified Media*. Berlin, Germany: Springer, 2009.

[33] J. R. Mosig and F. E. Gardiol, "A dynamic radiation model for microstrip structures," in *Advances in Electronics and Electron Physics*, vol. 59, P. W. Hawkes, Ed. New York: Academic, 1982, pp. 139–237.

[34] J. R. Mosig, "Integral equation technique," in *Numerical Techniques for Microwave and Millimeter-Wave Passive Structures*, T. Itoh, Ed. New York: Wiley, 1989, pp. 133–213.

[35] K. A. Michalski, "The mixed-potential electric field integral equation for objects in layered media," *Arch. Elek. Ubertragung.*, vol. 39, no. 5, pp. 317–322, Sep./Oct. 1985.

[36] K. A. Michalski and J. R. Mosig, "Multilayered media Green functions in integral equation formulations," *IEEE Trans. Antennas Propag.*, vol. 45, no. 3, pp. 508–519, Mar. 1997.

[37] D. C. Kuo, H. H. Chao, J. R. Mautz, B. J. Strait, and R. F. Harrington, "Analysis of radiation and scattering by arbitrary configurations of thin wires," *IEEE Trans. Antennas Propag.*, vol. 20, no. 6, pp. 814–815, Nov. 1972.

[38] L. Grcev, F. Rachidi, and V. A. Rakov, "Comparison of electromagnetic models of lightning return strokes using current and voltage sources," in *Proc. 12th Int. Conf. Atmospheric Elect.*. Versailles, France, 2003, pp. 593–596.

[39] EM Software and Systems-S.A. (Pty) Ltd., FEKO, Stellenbosch, South Africa, [Online]. Available: http://www.feko.info

[40] D. L. Jones and C. P. Burke, "The DC field components of horizontal and vertical electric dipole sources immersed in three stratified media," *Ann. Geophys.*, vol. 15, no. 4, pp. 503–510, 1997.

[41] A. Poggio, R. Bevensee, and E. K. Miller, "Evaluation of some thin wire computer programs," *IEEE Antennas Propag. Symp.*, vol. 12, pp. 181–184, Jun. 1974.

[42] J. M. Myers, S. S. Sandler, and T. T. Wu, "Electromagnetic resonances of a straight wire," *IEEE Trans. Antennas Propag.*, vol. 59, no. 1, pp. 129–1134, Jan. 2011.

Vesna Arnautovski-Toseva (M'89) was born in Zagreb, Croatia, in 1961. She received the Dipl.Ing., M.S., and Ph.D. degrees in electrical engineering from the Saints Cyril and Methodius University, Skopje, Macedonia.

Since 1989, she has been serving on the Faculty of Electrical Engineering and Information Technologies, Saints Cyril and Methodius University, Skopje, where she is currently an Associate Professor. She is also with the Laboratoire des Sciences et Matériaux pour l'Electronique et, d'Automatique, Blaise Pascal University, Clermont-Ferrand, France. Her research interests include electromagnetic compatibility (EMC), computational electromagnetics applied to high frequency and transient grounding, lightning, and EMC in power line communications.

Dr. Arnautovski-Toseva is a member of the Macedonian CIGRE Study Committee C3.

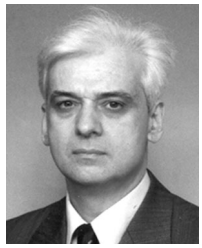

Leonid Grcev (M'84–SM'97) was born in Skopje, Macedonia, in 1951. He received the Dipl.Ing. degree from the Saints Cyril and Methodius University, Skopje, Macedonia, and the M.S. and Ph.D. degrees from the University of Zagreb, Zagreb, Croatia, all in electrical engineering.

He is currently a Professor with the Faculty of Electrical Engineering and Information Technologies, Saints Cyril and Methodius University, Skopje, where he has also held the positions of an Assistant Professor, Associate Professor, and Vice Dean since 1988. From 1978 to 1988, he was with the Telecommunications Department, Electric Power Company, Macedonia, Skopje. He has been a Visiting Professor at the Technical University of Aachen, Aachen, Germany; the Eindhoven University of Technology, Eindhoven, The Netherlands; and the Swiss Federal Institute of Technology, Lausanne, Switzerland. He was responsible for several international projects related to electromagnetic compatibility (EMC). He is the author or coauthor of many scientific papers published in peer-reviewed journals and presented at international conferences. His research interests include EMC, high frequency and transient grounding, lightning and EM-field health effects.

Dr. Grcev is a member of the CIGRE Working Groups related to EMC and lightning protection and has served as the Chairperson and as a member of scientific committees at international conferences. He is a member of the Macedonian Academy of Sciences and Arts.